Materials and Structures, 1992, **25**, 201–211

Strengthening of RC beams with epoxy-bonded fibre-composite materials

T. C. TRIANTAFILLOU, N. PLEVRIS

Department of Civil Engineering, Massachusetts Institute of Technology, Cambridge, MA 02139, USA

Strengthening of concrete beams with externally bonded fibre-reinforced plastic (FRP) materials appears to be a feasible way of increasing the load-carrying capacity and stiffness characteristics of existing structures. FRP-strengthened concrete beams can fail in several ways when loaded in bending. The following collapse mechanisms are identified and analysed in this study: steel yield–FRP rupture, steel yield–concrete crushing, compressive failure, and debonding. Here we obtain equations describing each failure mechanism using the strain compatibility method, concepts of fracture mechanics and a simple model for the FRP peeling-off debonding mechanism due to the development of shear cracks. We then produce diagrams showing the beam designs for which each failure mechanism is dominant, examine the effect of FRP sheets on the ductility and stiffness of strengthened components, and give results of four-point bending tests confirming our analysis. The analytical results obtained can be used in establishing an FRP selection procedure for external strengthening of reinforced concrete members with lightweight and durable materials.

NOTATION

A	Area
A_s	Area of steel reinforcement
a	Crack length
b	Width of cross-section
b_{fc}	Width of fibre-composite sheet
C	Compliance
c	Distance from extreme compressive fibre to neutral axis
d	Effective depth
E	Young's modulus
E_c	Young's modulus of concrete
E_{fc}	Young's modulus of fibre-composite
E_s	Young's modulus of steel
f_c	Stress in concrete
f'_c	Compressive strength of concrete
f_{fc}	Stress in fibre-composite
f_r	Modulus of rupture for concrete
f_s	Stress in steel
f_y	Yield stress of steel
G	Shear modulus
G_{fc}	Shear modulus of fibre-composite
G_s	Shear modulus of steel
G_{II}	Mode II strain energy release rate
G_{IIC}	Critical mode II strain energy release rate
h	Height of cross-section
I	Moment of inertia
k	Constant
M	Bending moment
M_{cr}	Bending moment at first cracking
M_u	Ultimate bending moment
M_y	Bending moment at first yield
P	Load
t	Thickness of fibre-composite
U	Strain energy
u	Displacement
V	Shear force
v	Vertical crack opening displacement
w	Horizontal crack opening displacement
$\bar{y}$	Depth of centroid of the concrete stress block
β_1	Constant used to define the depth of the equivalent rectangular stress block
ε_c	Strain in concrete
ε_c^t	Strain at concrete top fibre
ε_{fc}	Strain in fibre-composite
ε_{fc}^*	Uniaxial strain of fibre-composite at failure
ε_0	Initial strain at extreme tensile fibre of concrete
ε_s	Strain in steel
λ	Constant
ρ_{fc}	Area fraction of fibre-composite
ρ_{fc}^l	Lower limit of fibre-composite area fraction
ρ_{fc}^u	Upper limit of fibre-composite area fraction
ρ_s	Area fraction of steel reinforcement
ϕ	Curvature
ϕ_{cr}	Curvature at first cracking
ϕ_u	Ultimate curvature
ϕ_y	Curvature at first yield

0025-5432/92

1. INTRODUCTION

The maintenance, rehabilitation and upgrading of structural members is as important and technical as the design and construction of new ones. Upgrading usually involves strengthening of existing members to carry higher ultimate loads and/or satisfy more stringent serviceability requirements. Strengthening of reinforced concrete members *in situ* by externally bonding steel plates using epoxy resins has been recognized to be an effective and convenient method of improving their performance under loads. The technique has been used widely for both bridges and buildings and for concrete surfaces in the tension and compression zones (e.g. [1–8]).

Strengthening through external bonding of steel plates has the following disadvantages: (a) difficulty in manipulating the plates at the construction site; (b) deterioration of the bond at the steel–concrete interface caused by the corrosion of steel; and (c) proper formation of joints, due to the limited delivery lengths of the steel plates. These difficulties have led to the idea of replacing the steel plates by fibre-reinforced composite sheets made of unidirectional, continuous fibres such as glass, carbon and Kevlar, bonded together with a matrix such as epoxy resin [9–12].

In this paper, we focus on developing a basic understanding of the flexural behaviour of reinforced concrete (RC) beams strengthened with externally bonded fibre-reinforced plastic (FRP) materials. We examine the influence of FRP plates on the failure mechanisms, the ductility and the stiffness of strengthened beams, develop equations describing the failure load for each failure mechanism, produce diagrams showing the beam designs for which each failure mechanism is dominant, and give the results of four-point bending experiments confirming our analysis. The analytical results obtained are useful in establishing an FRP material selection procedure for external strengthening of RC members.

2. BACKGROUND

The technique of bonding steel plates to the surfaces of concrete members has been widely used in practice. Early research work established the static performance of beams and slabs with steel plates as tensile and shear reinforcement [1,13,14]. Results on the behaviour of large RC beams with bonded steel plates have been reported by Irwin [2] and Macdonald [15]. Jones *et al.* [16,17] conducted extensive experimental work on the use of external reinforcement in the form of steel plates glued to the tension face of plain and reinforced concrete beams in bending. Ladner [18] derived a set of lower and upper limits for the total reinforcement ratio (internal and external) to ensure that it will yield before the concrete will fail in the compression zone. A series of comprehensive test data on the effect of plate thickness, glue thickness, layered plates, variations in glue thickness and the presence of stress concentrations in the adhesive layer were presented in a study by Swamy *et al.* [8]. From the analysis standpoint, the above studies verified the validity of the strain compatibility method for the prediction of the failure loads, and concluded that external steel sheets can be treated in a manner similar to conventional longitudinal reinforcement. The study of the failure mechanisms of concrete beams with steel plates in the tension zone reveals the important role of bond failure (delamination) in member performance. In the design of strengthened concrete beams, bond failure needs to be considered in addition to the mechanisms of concrete crushing and steel yielding.

Saadatmanesh and Ehsani [11] reported preliminary results from the study of RC beams with glass fibre-reinforced plastic (GFRP) sheets bonded on the tension zone. Their work emphasizes that selection of the appropriate adhesive is of primary importance in the mechanical performance of the strengthened members. Carbon fibre-reinforced plastic composites (CFRP) were successfully employed for the first time in loading tests for strengthening of beams by Kaiser [12]. His work shows the validity of the strain compatibility method in the analysis of cross-sections, and suggests that possible development of shear cracks may lead to a peeling-off of the strengthening sheet. Kaiser's study includes the development of an analytical model for the composite plate anchoring which is in good agreement with his experimental results.

In this paper, the authors use the strain compatibility method, concepts of fracture mechanics and a simple model for the FRP peeling-off mechanism to provide a systematic approach to the study of the short-term flexural behaviour of RC beams strengthened with externally bonded composite sheets. The analysis assumes singly reinforced concrete members with rectangular cross-sections; in principle, similar approaches apply for other geometric configurations.

3. ANALYSIS

A typical concrete beam strengthened with FRP sheet is shown in Fig. 1. The shear capacity of the member is not of concern in this work. The fibre-composite plate has width b_{fc}, thickness t, Young's modulus E_{fc} and tensile failure strain ε^*_{fc}; the concrete has compressive strength f'_c and Young's modulus E_c; and the steel reinforcement has area A_s, Young's modulus E_s and yield stress f_y. The assumed stress–strain relationships for the three materials are shown in Fig. 2. Further assumptions are that plane sections before bending remain plane after bending and that the tensile resistance of the concrete and the adhesive may be neglected.

FRP-strengthened concrete beams can fail in several ways when loaded in bending. If both the steel and the FRP area fractions of the section are quite small, steel yielding may be followed by rupture of the composite sheet. If the FRP area fraction of the section is high, failure is due to concrete crushing while the steel may have

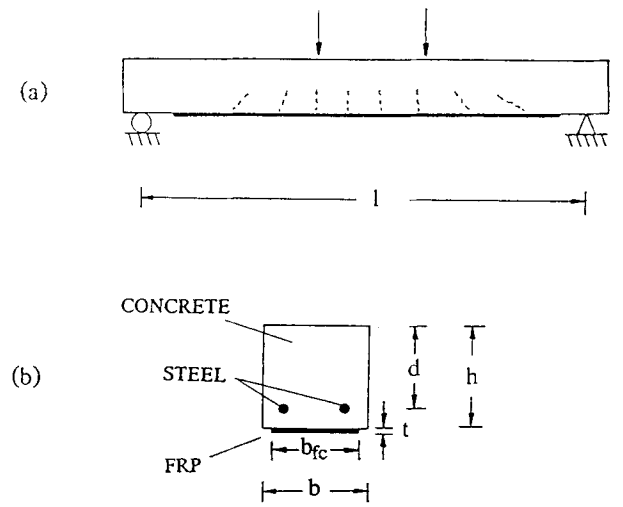

Fig. 1 (a) A concrete beam of span l strengthened with FRP sheet; (b) the cross-section of the beam in (a).

yielded or not, depending on its area fraction. Finally, the bond, too, between the FRP and the concrete, may fail. Debonding may occur due to: (a) the sudden propagation of cracks in the adhesive (most resin adhesives are brittle); (b) peeling-off of the FRP sheet because of shear cracks in the concrete; and (c) shear failure of the concrete layer between the FRP sheet and the longitudinal reinforcement.

3.1 Steel yield–FRP rupture, steel yield–concrete crushing and compression failure mechanisms

A cross-section when the flexural strength is reached due to yielding of the steel reinforcement followed by rupture of the composite laminate appears in Fig. 3a. Note that the strain distribution allows for an initial strain, ε_0, at the concrete bottom fibre; it is the result of applied loads at the time when the strengthening process (external bonding of FRP) occurs. When the FRP sheet is thick enough and the steel area fraction of the section is small, yielding of the steel will be followed by compressive crushing of the concrete when the strain in the extreme compression fibre equals 0.003 (Fig. 3b). Finally, if the steel area fraction and/or the FRP area fraction of the section is high, the concrete will reach its maximum capacity before the steel yields and before the composite sheet ruptures. Again, the flexural strength is reached when the strain at the extreme compression fibre of the concrete is 0.003 (Fig. 3c). Equilibrium of forces can be used to obtain the neutral axis depth, c/d, and the ultimate moment capacity for the three failure mechanisms is as follows.

For *steel yield–FRP rupture*:

$$\frac{M_u}{bd^2 f'_c} = \frac{f_y}{f'_c}\rho_s\left(1 - \frac{\bar{y}}{d}\right) + \frac{E_{fc}\varepsilon^*_{fc}}{f'_c}\rho_{fc}\left(\frac{h}{d} - \frac{\bar{y}}{d}\right) \quad (1)$$

For *steel yield–concrete crushing*:

$$\frac{M_u}{bd^2 f'_c} = 0.85\beta_1\frac{c}{d}\left(\frac{h}{d} - \frac{\beta_1 c}{2d}\right) - \frac{f_y}{f'_c}\rho_s\left(\frac{h}{d} - 1\right) \quad (2)$$

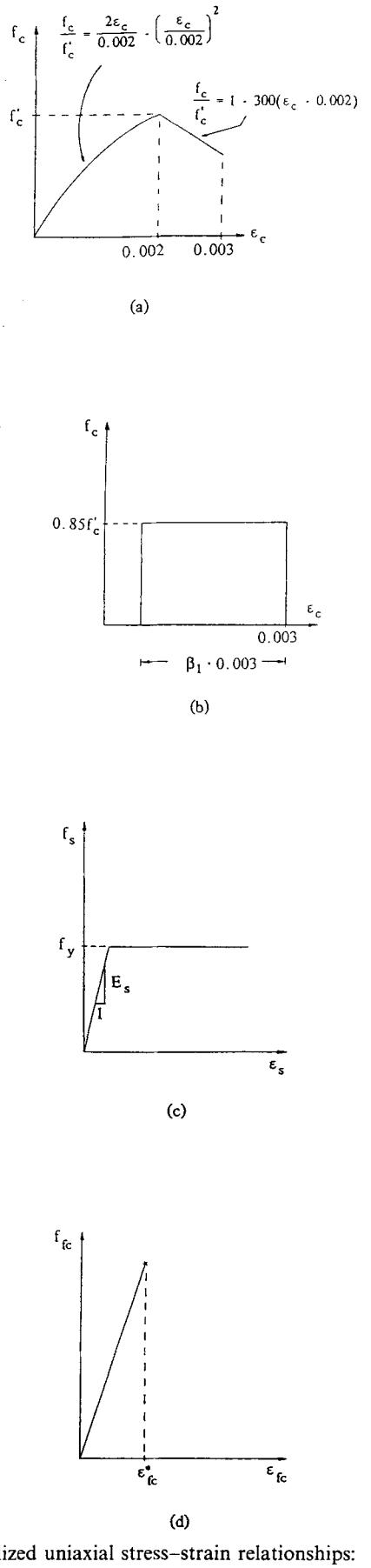

Fig. 2 Idealized uniaxial stress–strain relationships: (a) concrete in compression (based on Kent and Park's [19] model), (b) equivalent rectangular concrete block at failure, (c) steel, (d) fibre-composite.

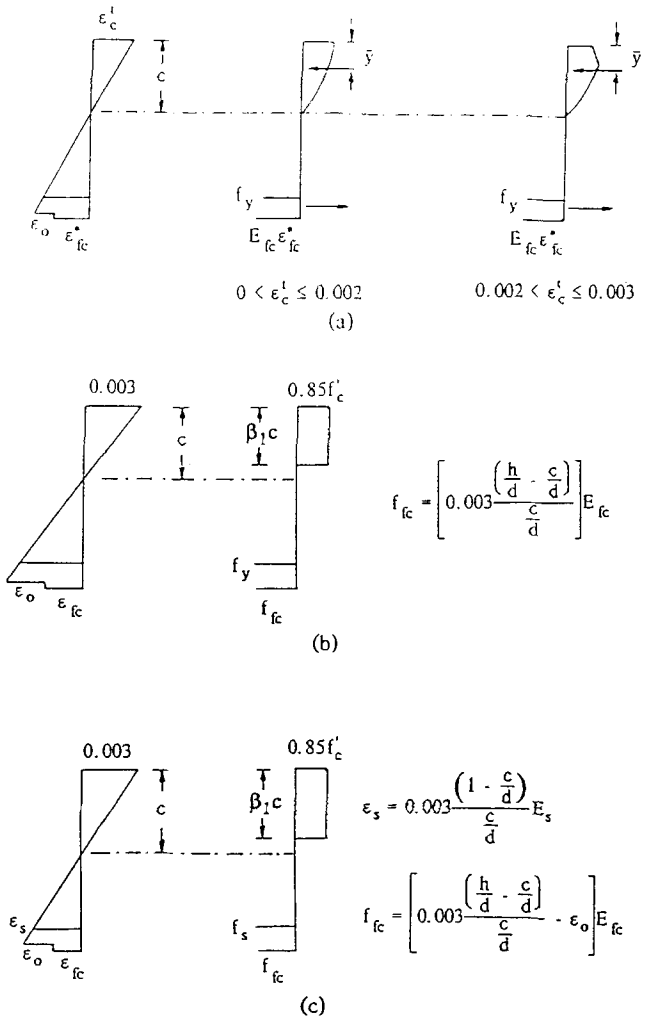

Fig. 3 Strain and stress distribution at a section when the flexural strength is reached: (a) steel yield–FRP rupture, (b) steel yield–concrete crushing, (c) compression failure.

For *compression failure*:

Equation 2 with f_y replaced by $\dfrac{0.003[1 - (c/d)]}{c/d}E_s$ (3)

where $\rho_s = A_s/bd$, $\rho_{fc} = b_{fc}t/bd$ and $\bar{y}$ in Equation 1 is the distance from the centroid of the concrete stress distribution to the top fibre; it can be determined in terms of ε^*_{fc}, ε_0, h/d and c/d (described in terms of ε^*_{fc}, ε_0, h/d, ρ_s, ρ_{fc}, f_y, f'_c and E_{fc}).

3.2 Debonding

3.2.1 *Interface crack propagation*

The bond between the composite sheet and the concrete may fracture in a sudden manner as the result of the catastrophic propagation of a crack along the FRP–concrete interface. Possible reasons for the existence of such a crack are: (a) imperfections in the spreading of the adhesive; (b) flexural cracking in the concrete, resulting in horizontal interface cracks developed from the bottom tip of the flexural cracks; (c) peeling-off of the composite when the concrete tensile face is not perfectly flat; and (d) fatigue loads.

While the composite sheet is loaded in tension, the adhesive is loaded primarily in shear, providing the necessary shear connection between the concrete and the composite. It follows that the crack propagation mode will resemble fracture mode II. Here, the problem of the propagation of an interface crack is treated by considering the relationship between the strain energy release rate required for crack propagation and the compliance of a member. The compliance method is described by Knott [20] and has been used by Anandarajah and Vardy [21] to analyse the interfacial shear fracture of 'open sandwich beams' (plain concrete members reinforced with externally bonded steel plates) in conjunction with a finite-element procedure. Similar techniques for analysing interfacial delamination based on the strain energy release rate exist: the method of Triantafillou and Gibson [22] is based on the volume of material that is unloaded by crack propagation; and that of Hamoush and Ahmad [23] employs calculation of the J-integral using the finite-element method.

In the compliance method, the strain energy release rate, G_{II}, for in-plane shear delamination satisfies the condition

$$G_{II} = \frac{kP^2}{b}\left(\frac{\partial C}{\partial a}\right) \tag{4}$$

where b is the width of the member, P is the applied load, a is the crack length, k is a constant and C is the reciprocal of the gradient of the load–deflection curve, i.e.

$$C = u/P \tag{5}$$

where u is the displacement under the load P. The constant k relates the load and displacement to the strain energy U as follows:

$$U = kPu \tag{6}$$

Note that $\partial C/\partial a$ in Equation 4 depends on the applied load P. For a particular value of P the relationship between the compliance, C, and the crack length, a, can be established by analysing the beam using a finite-element procedure. The gradient $\partial C/\partial a$ corresponding to any particular crack length is then obtained and the strain energy release rate G_{II} calculated. Fracture occurs when the strain energy release rate equals the critical strain energy release rate for the interface, G_{IIC}:

$$G_{IIC} = \frac{kP^2}{b}\left(\frac{\partial C}{\partial a}\right) \tag{7}$$

The load causing debonding is then calculated from Equation 7. The critical strain energy release rate for the interface, G_{IIC}, can be measured using double-shear specimens pulled in tension [22].

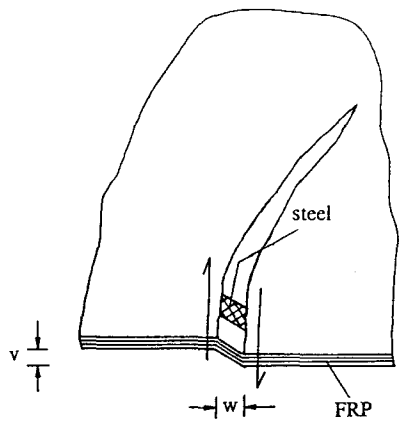

Fig. 4 Vertical and horizontal concrete crack openings resulting in FRP peeling-off.

3.2.2 *FRP peeling-off*

Shear cracks in concrete beams are associated with both horizontal and vertical openings, primarily due to the dowel action and aggregate interlock mechanisms (see Fig. 4). For the same area fraction and spacing of shear reinforcement (steel stirrups) the crack opening is controlled by the area fractions of the longitudinal steel reinforcement and the FRP sheet through the dowel mechanism. In a first attempt to model the phenomenon we assume that the dowel deformations in the longitudinal steel and the FRP at the crack location are primarily due to shear. Therefore, a certain percentage of the shear force V at a cross-section is equal to the shear strain, v/w (ratio of the vertical to the horizontal crack opening), multiplied by the total shear stiffness of the steel reinforcement and the FRP sheet, $\sum GA$ ($\sum GA = G_s A_s + G_{fc} b_{fc} t$; G_s and G_{fc} are the shear modulus of steel and FRP, respectively). Thus, we can write

$$V \propto \frac{v}{w} \sum GA \tag{8}$$

Peeling-off of the FRP will occur when the ratio v/w reaches a critical value, $(v/w)_{cr}$, which is a characteristic property of the FRP–concrete bond. Moreover, the shear force, V, is proportional to the external load, P. Hence, delamination due to FRP peeling-off will initiate at the location of a shear crack when

$$P \propto \left(\frac{v}{w}\right)_{cr} \sum GA \tag{9}$$

Equation 9 describes the debonding load as a linear function of the shear stiffness:

$$P = \lambda \sum GA \tag{10}$$

Finally, Equation 10 can be calibrated from tests on beams by varying the shear stiffness $\sum GA$ and recording the debonding load. The approach presented here is expected to yield reasonable results only when the area fractions of steel and FRP are relatively high, in which case the dowel force is primarily carried by shearing of these materials.

3.2.3 *Concrete shear delamination*

Another FRP–concrete separation mechanism involves shear failure of the concrete layer between the FRP sheet and the steel reinforcement. Debonding in this case initiates near the ends of the FRP sheet (anchorage zone) due to high interface shear stresses; it occurs when the peak value of the interface shear stress reaches a limiting value which depends on the strength of concrete, f'_c. This limiting value is approximately 8 MPa for normal-strength concrete [9,12,24]. The detailed analysis for this mechanism can be found in Kaiser [12].

4. FIBRE-COMPOSITE MATERIAL SELECTION

This section addresses issues related to determining which composite material is the most appropriate and how much of it is needed to upgrade an existing member to a specified moment and/or stiffness capacity. Useful information for the material selection process can be obtained by examining the influence of the composite sheet on the member's failure mechanism, ultimate capacity, ductility and stiffness characteristics.

4.1 Failure diagrams

Without considering debonding, the ultimate bending capacity of a member is described by Equations 1–3. The beam design at which two failure mechanisms occur simultaneously is found by equating the associated equations. Treating the reinforcement ratios ρ_{fc} and ρ_s as variables, one obtains the diagram shown in Fig. 5, which illustrates how the failure mechanism depends on the quantity of the external FRP reinforcement. In this diagram

$$\rho_{fc1} = \frac{0.00255\beta_1 f'_c}{(0.003 + \varepsilon^*_{fc} + \varepsilon_0)E_{fc}} \left(\frac{h}{d}\right)\left(\frac{1}{\varepsilon^*_{fc}}\right)$$

$$\rho_{fc2} = 0.00255\beta_1 f'_c \left[\left(0.003 + \frac{f_y}{E_s}\right)^2 \times E_{fc}\left(\frac{h}{d} - \frac{0.003}{0.003 + (f_y/E_s)}\right) - \left(0.003 + \frac{f_y}{E_s}\right)E_{fc}\varepsilon_0\right]^{-1}$$

$$\rho_{s1} = \frac{0.00255\beta_1 f'_c}{(0.003 + \varepsilon^*_{fc} + \varepsilon_0)f_y} \frac{h}{d}$$

$$\rho_{s2} = 0.00255\beta_1 f'_c \left[\left(0.003 + \frac{f_y}{E_s}\right)f_y\right]^{-1}$$

The same diagram is produced in Fig. 6 for three types of unidirectional composite: CFRP, Kevlar FRP (KFRP) and GFRP; the composite material properties are listed in Table 1. Fig. 8 and all subsequent figures in this section are based on the following material properties and geometric parameters: $f'_c = 34.5$ MPa, $E_s = 200$ GPa, $f_y = 414$ MPa, $h/d = 1.1$, $\varepsilon_0 = 0.0008$. As Fig. 6 illustrates, it is very unlikely that the failure mechanism will involve failure of the FRP sheet when glass or Kevlar fibres are employed; the ultimate strain for these fibres is much

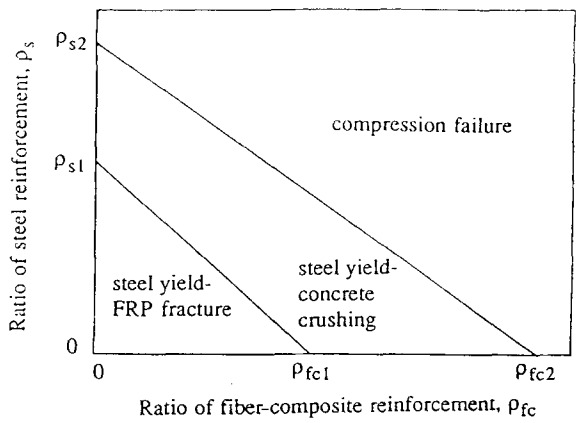

Fig. 5 Influence of the FRP and steel reinforcement on the failure mechanism.

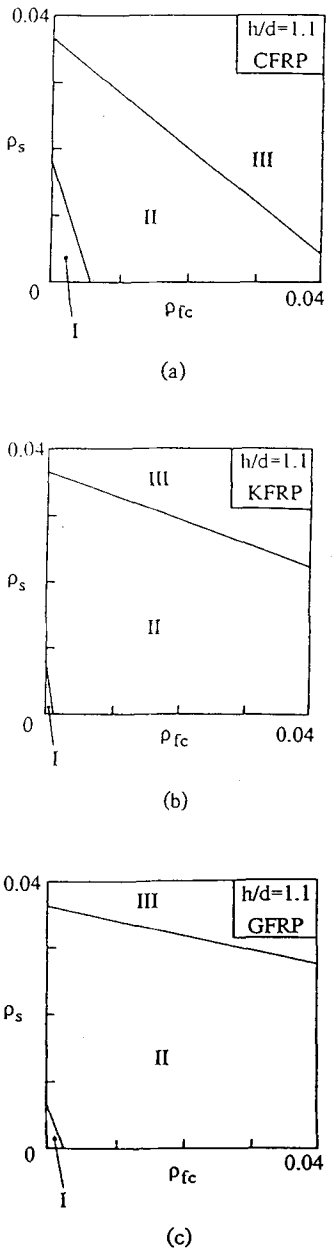

Fig. 6 Failure diagrams for different composite sheets: (a) CFRP, (b) KFRP, (c) GFRP. I, Steel yield–FRP fracture. II, Steel yield–concrete crushing. III, Compression failure.

Table 1 Composite material properties[a]

Material	Young's modulus, E_{fc} (GPa)	Ultimate strain
Carbon FRP (CFRP)	186	0.0075
Kevlar FRP (KFRP)	83	0.0250
Glass FRP (GFRP)	51	0.0250

[a] The values listed do not refer to any specific material combinations; they represent typical properties useful in performing parametric studies.

higher than that for carbon fibres. Hence, a ductile behaviour is expected in this case.

The important effect of the type and area fraction of FRP on the ultimate bending capacity of post-strengthened members is illustrated in Fig. 7; the beneficial effect of the fibre-composite sheets is more pronounced for small ratios of steel reinforcement (Fig. 7, dashed lines). Furthermore, the increase in bending capacity becomes rather insignificant when failure is governed by compressive crushing of the concrete. It is recommended that the area fraction of composite material corresponding to the transition from the steel yield–concrete crushing mode to the compressive mode be an upper limit to the external FRP reinforcement. The FRP reinforcement ratio at this transition is

$$\rho_{fc}^{u} = \left(\frac{0.00255\beta_1 f'_c}{[0.003 + (f_y/E_s)]} - f_y\rho_s\right)\left\{\left[\left(0.003 + \frac{f_y}{E_s}\right) \times \left(\frac{h}{d} - \frac{0.003}{[0.003 + (f_y/E_s)]}\right) - \varepsilon_0\right]E_{fc}\right\}^{-1} \quad (11)$$

Moment capacity versus external FRP reinforcement ratio curves similar to those presented in Fig. 7 can be used for the selection of the type and area fraction of fibre-composite needed to upgrade an existing structural component.

4.2 Ductility

An appropriate ductility measure is given by the ratio of the curvature at failure, ϕ_u, to the curvature at first yield of the steel reinforcement, ϕ_y. The curvature ductility ratio can be established by moment–curvature curves idealized as trilinear (Fig. 8). The quantities needed to define the M–ϕ relationship are calculated using the strain compatibility method as follows.

For *cracking*:

$$\frac{M_{cr}}{bd^2 f'_c} = \frac{f_r}{6f'_c}\left(\frac{h}{d}\right)^2 \qquad \phi_{cr}d = \frac{2f_r}{E_c(h/d)} \quad (12)$$

where f_r is the modulus of rupture for concrete, M_{cr} is the moment required to cause cracking of the cross-section and ϕ_{cr} is the curvature at first cracking. Equations 12 are based on the assumption that the

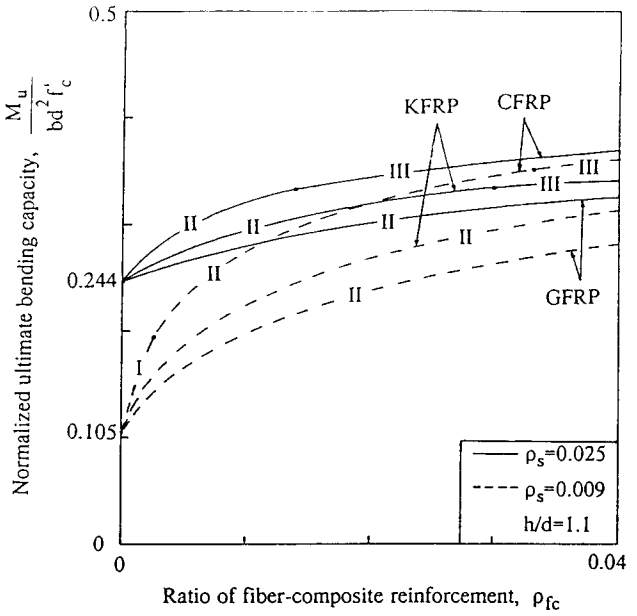

Fig. 7 Dependence of the ultimate bending capacity on the ratio of external reinforcement for CFRP, KFRP and GFRP composite sheets. I, Steel yield–FRP fracture. II, Steel yield–concrete crushing. III, Compression failure.

fibre-composite has a negligible effect on the cracking moment; the assumption is quite realistic for small composite sheet area fractions.

For *steel first yield*:

$$\frac{M_y}{bd^2f'_c} = \left(1 - \frac{\bar{y}}{d}\right)\frac{f_y\rho_s}{f'_c} + \left(\frac{h}{d} - \frac{\bar{y}}{d}\right)\frac{E_{fc}\rho_{fc}}{f'_c} \times \left(\frac{[(h/d) - (c/d)]}{[1 - (c/d)]}\frac{f_y}{E_s} - \varepsilon_0\right) \quad (13)$$

$$\phi_y d = \frac{f_y}{E_s[1 - (c/d)]}$$

where c/d, the depth of the neutral axis, is obtained from the condition of force equilibrium at the cross-section when the steel first yields. The distance from the centroid of the concrete stress distribution to the top fibre, $\bar{y}$, in Equations 13 is determined in terms of f_y/E_s and c/d.

For *ultimate capacity–FRP rupture*:

$$\frac{M_u}{bd^2f'_c} \text{ is described by Equation 1} \qquad \phi_u d = \frac{\varepsilon^*_{fc} + \varepsilon_0}{(h/d) - (c/d)} \quad (14)$$

For *ultimate capacity–concrete crushing*:

$$\frac{M_u}{bd^2f'_c} \text{ is described by Equation 2} \qquad \phi_u d = \frac{0.003}{c/d} \quad (15)$$

The character of typical moment–curvature relationships for sections of members strengthened with FRP composites is illustrated in Fig. 8 (material properties are

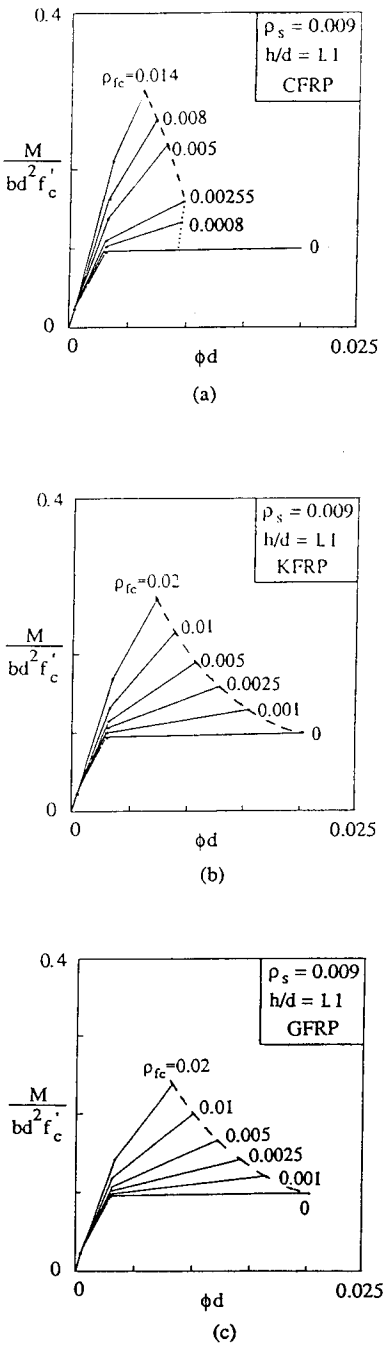

Fig. 8 Moment–curvature relationships for various FRP composite reinforcement ratios: (a) CFRP, (b) KFRP, (c) GFRP. (– – –) Concrete crushing. (· · · ·) FRP rupture.

as described earlier, the modulus of rupture for concrete is taken as f_r = 3.7 MPa and the steel reinforcement ratio is assumed to be ρ_s = 0.009). Note that when most of the member's resistance comes from the FRP, very low ductility exists. The effect of the FRP reinforcement ratio, ρ_{fc}, on the ductility of the member is better shown in Fig. 9 for a wide range of steel reinforcement ratios, ρ_s. The ductility increases as ρ_{fc} decreases, unless ρ_{fc} becomes small enough so that failure is characterized by FRP rupture. The fibre-composite ratio at the transition from the steel yield–concrete crushing mode to the steel

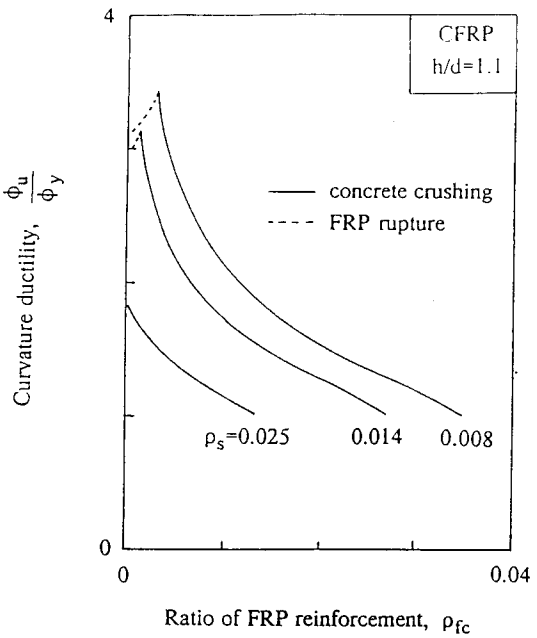

Fig. 9 Curvature ductility ratio as a function of CFRP reinforcement ratio for various amounts of steel reinforcement.

yield–FRP rupture mode is given by

$$\rho_{fc}^{l} = \left[\frac{0.00255\beta_1 f_c'}{(0.003 + \varepsilon_{fc}^{*} + \varepsilon_0)}\left(\frac{h}{d}\right) - f_y\rho_s\right](E_{fc}\varepsilon_{fc}^{*})^{-1} \quad (18)$$

This ratio could be regarded as a lower limit in the FRP material selection process to assure non-catastrophic failures. However, as Fig. 9 illustrates, the decrease in ductility for $\rho_{fc} < \rho_{fc}^{l}$ is rather insignificant and a lower limit to the composite reinforcement ratio does not seem justifiable. A comparison of the performance of the three types of composite materials in terms of ductility is presented in Fig. 10 for $\rho_s = 0.014$. Note that unless failure is governed by FRP rupture, the results of Fig. 10 by no means indicate that GFRP and KFRP should be preferred to CFRP for ductility considerations: the GFRP or KFRP reinforcement ratio needed to achieve a given moment capacity is much higher than that when CFRP composite is used (the materials have different elastic moduli).

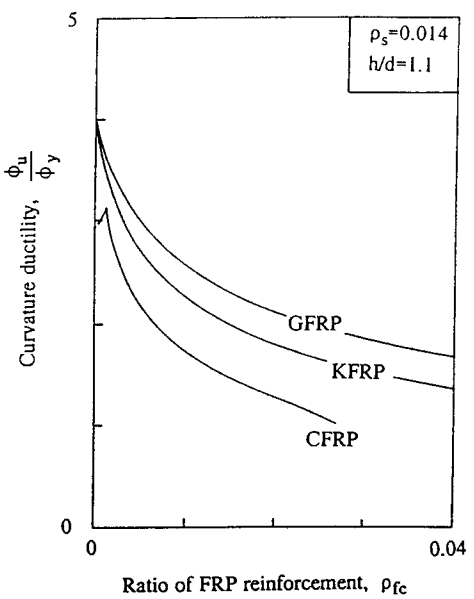

Fig. 10 Curvature ductility versus FRP reinforcement ratio for three types of externally bonded composite sheets.

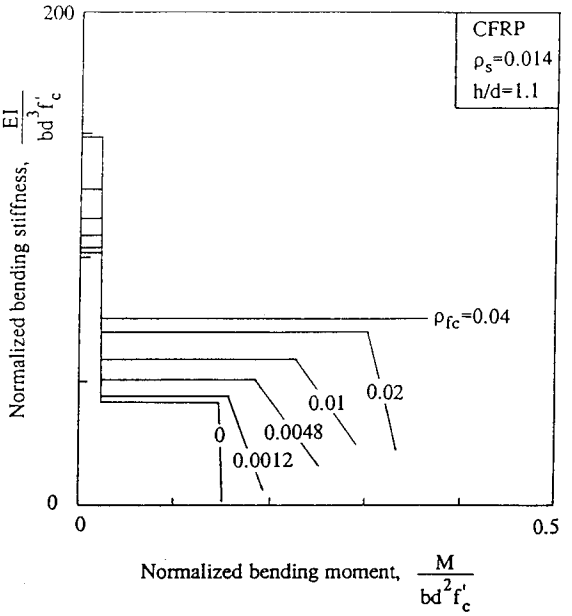

Fig. 11 The effect of the fibre-composite reinforcement ratio on the bending stiffness of CFRP-strengthened members.

4.3 Stiffness

Using the incremental equation $EI = \Delta M/\Delta\phi$ and the moment–curvature relationships obtained earlier, the bending stiffness, EI, can be established as a function of the bending moment, M. Typical EI–M relationships are shown in Fig. 11 for $\rho_s = 0.014$ and various CFRP composite reinforcement ratios. Bending stiffness–moment relationships such as those of Fig. 11 can be used for the calculation of deflections and for the selection of the composite reinforcement ratio, ρ_{fc}, when the composite material is used for stiffness upgrading.

5. EXPERIMENTAL PROGRAMME

Eight concrete beams were constructed and tested in four-point bending to study the effect of the FRP area fraction on the failure mechanism, ultimate moment capacity and stiffness of the strengthened member. Seven of the beams were strengthened with unidirectional CFRP plates; one beam was used as a control specimen. Three 100 mm × 200 mm concrete cylinders were also cast and tested when the beams were tested to determine the compressive strength of the concrete.

The cement:sand:gravel proportions in the concrete mix were 1:2:3 by weight and the water/cement ratio was 0.55. Type I Portland cement was used and the maximum size of the aggregate was 10 mm. Following

Table 2 CFRP area fraction of beams tested

Beam No.	CFRP thickness (mm)	CFRP width, b_{fc} (mm)	CFRP area fraction
1	–	–	–
2	0.20	42.6	0.0009
3	0.20	60.5	0.0013
4	0.65	63.2	0.0043
5	0.65	63.2	0.0043
6	0.90	63.3	0.0059
7	0.90	63.3	0.0059
8	1.90	63.9	0.0126

Table 3 Properties of materials used in experimental programme

Material	Young's modulus (GPa)	Strength (MPa)
Concrete	31.6	44.7 (f'_c)
Steel	200	517 (f_y)
CFRP	186	1450[a] ($E_{fc}\varepsilon^*_{fc}$)

[a] Tensile strength. Strain at failure $\varepsilon^*_{fc} = 0.0078$.

casting the specimens were covered by wet plastic bags. After 24 h the moulds were removed and the specimens were cured under water at 20°C for 7 days; the specimens were left then to air-dry in the laboratory. The CFRP sheets were epoxy-bonded to the tension face of the beams 24 days after the moulds were removed. The adhesive was applied to both the CFRP and the concrete surfaces in two steps. First, a low-viscosity epoxy was applied to the concrete and cured for 6 h. Then, a high-viscosity epoxy was applied to both the concrete and the CFRP sheet and cured for 3 days to attain its maximum strength. Before applying the epoxy the concrete surface was roughened by a metallic brush and both the concrete and the CFRP surfaces were cleaned. All specimens were tested when the concrete was at an age of 28 days.

Each beam had a cross-section of 76 mm × 127 mm and was 1350 mm long. All the beams were reinforced with two 4.6 mm diameter bars; the effective depth was 111 mm. The shear reinforcement consisted of 4.6 mm diameter stirrups placed at 40 mm spacing. The CFRP sheets were 1070 mm long. The fibre-composite material consisted of high-modulus carbon fibres at a volume fraction of 65%, bonded together with an epoxy matrix. The CFRP area fraction for each of the eight beam designs is given in Table 2, and a summary of the material properties used in the experimental study is given in Table 3. Note that the properties of steel and CFRP were specified by the suppliers.

All the beams were loaded to failure, simply supported over a span of 1220 mm with equal point loads applied symmetrically with respect to the mid-span at a distance of 305 mm from each other. Load and deflection at 360 mm from the left-hand support were measured during the test with a load cell and a linear voltage differential transformer and were recorded on an X–Y recorder.

6. RESULTS AND DISCUSSION

Out of the eight beams tested, one failed by excessive yield of the steel reinforcement (this was the control specimen with $\rho_{fc} = 0$), two by steel yield–FRP rupture and five by debonding due to peeling-off of the composite. Table 4 lists the measured failure loads for each beam design tested, along with the failure mechanism. The results for the first three of the beams that failed by peeling-off of the FRP were used to calibrate Equation 10. The ultimate load for these beams was plotted against the shear stiffness of the longitudinal steel + FRP reinforcement (the shear modulus of CFRP was 4.4 GPa) and the data suggested that the constant λ (see Equation 10) be approximately 0.011. The load–deflection curves for the remaining five beam designs are shown in Fig. 12.

Table 4 Measured failure loads for FRP-strengthened beams

ρ_{fc}	Failure load (kN)	Failure mechanism
–	8.59	Under-reinforced RC beam
0.0009	13.16	Steel yield–FRP rupture
0.0013	17.27	Steel yield–FRP rupture
0.0043	29.56[a]	Debonding (FRP peeling-off)
0.0059	30.50[a]	Debonding (FRP peeling-off)
0.0059	27.90[a]	Debonding (FRP peeling-off)
0.0043	25.59	Debonding (FRP peeling-off)
0.0126	37.33	Debonding (FRP peeling-off)

[a] These test results were used to calibrate Equation 10.

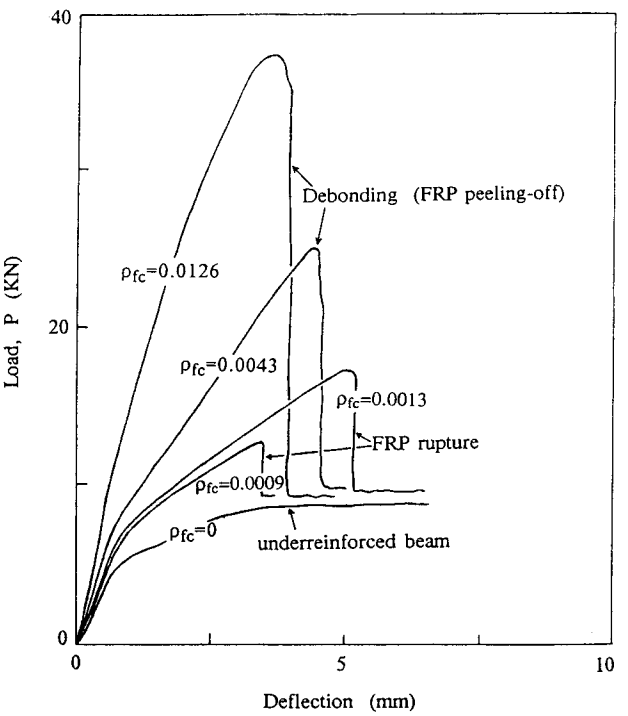

Fig. 12 Load–deflection curves for CFRP-strengthened concrete beams.

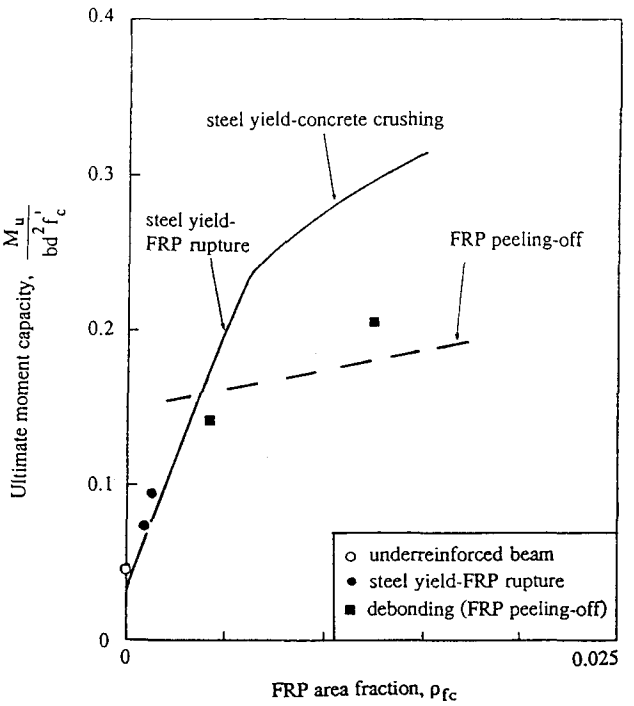

Fig. 13 Comparison between analysis (lines) and experimental results (data points) for the ultimate moment capacity and the failure mechanism of CFRP-strengthened concrete beams as a function of the composite sheet area fraction. $\rho_s = 0.00344$, $h/d = 1.14$.

Both FRP rupture and debonding due to peeling-off of the FRP produced a sudden drop in the load–deflection curves at a level corresponding to the response of the beam after yielding of the steel reinforcement. The peeling-off debonding failure took place in the epoxy adhesive used to bond the CFRP to the concrete.

A comparison between the limited experimental results obtained in this study (data points) and the analytical predictions (continuous and dashed lines) for the various failure mechanisms and the ultimate moment capacities is shown in Fig. 13; note that the test data used to calibrate Equation 10 are not used in the comparison. The overall agreement between theory and experiments is satisfactory.

In summary, the performance of all seven FRP-strengthened beams tested was superior to that of the beam without the FRP reinforcement, as far as the bending moment capacity and the stiffness are concerned. The failure mechanisms, however, of the strengthened members appear more 'catastrophic'.

7. CONCLUSIONS AND RECOMMENDATIONS

Strengthening of concrete beams with externally bonded composite sheets appears to be a feasible way of increasing the load-carrying capacity and stiffness characteristics of existing structures. The present study focused on establishing a systematic analysis procedure for the short-term flexural behaviour of FRP-strengthened members. The relevant failure mechanisms are: (a) steel yield–FRP rupture; (b) steel yield–concrete crushing; (c) compression failure; and (d) debonding either at the interface between the concrete and the FRP or through the concrete layer between the composite sheet and the steel reinforcement. Each failure mechanism was described by an equation giving the collapse load. The failure diagrams obtained give an overview of which collapse mechanism occurs for all possible steel + FRP reinforcement configurations. The limited test results obtained herein confirmed the analysis and emphasized the important role of cracking in the delamination of the composite sheet through a peeling-off mechanism; this mechanism was described by a simple model resulting in predictions consistent with the experimental findings. It appears that the FRP peeling-off debonding mechanism gives a limitation on the composite sheet thickness, beyond which brittle failure occurs without achieving the full flexural strength and ensuring ductility.

Before this novel strengthening technique can be applied in practice, studies must be performed to address additional issues such as the behaviour under sustained loading, fatigue, thermal cycling and humidity cycling. It is also to be remembered that the FRP–adhesive system has very low fire resistance unless the burning rate of the plastic materials is reduced either by use of additives or by chemical modification of the polymer chains. Nevertheless, the authors believe that the method of external reinforcement of concrete (and possibly of other materials such as wood) with advanced composites can be effective and economical, not only in rehabilitation applications but also in new constructions.

ACKNOWLEDGEMENT

The project was supported by a grant from the US Army Research Office through the Program for Advanced Construction Technology at MIT, for which we are grateful.

REFERENCES

1. Fleming, C. J. and King, G. E. M., 'The development of structural adhesives for three original uses in South Africa', in Proceedings of RILEM International Symposium on Synthetic Resins in Building Construction, Paris, 1967, pp. 75–92.
2. Irwin, C. A. K., 'The Strengthening of Concrete Beams by Bonded Steel Plates', TRRL Supplementary Report 160 UC (Transport and Road Research Laboratory, Department of the Environment, Crowthorne, UK, 1975, p. 8.
3. Hugenschmidt, H., 'Epoxy adhesive for concrete and steel', in Proceedings of 1st International Congress on Polymers in Concrete, London, 1976, pp. 195–209.
4. Dussek, I. J., 'Strengthening of Bridge Beams and Similar Structures by Means of Epoxy-Resin-Bonded External Reinforcement', Transportation Research Record No. 785 (1980) pp. 21–24.
5. Ryback, M., 'Reinforcement of bridges by gluing of reinforcing steel', *Mater. Struct.* **16**(91) (1981) 13–17.

6. Van Gemert, D. A., 'Repairing of concrete structures by externally bonded steel plates', in Proceedings of ICP/RILEM/IBK International Symposium on Plastics in Material and Structural Engineering, Prague, 1982, pp. 519–526.
7. Klaiber, F. W., Dunker, K. F., Wipf, T. J. and Sanders, W. W., Jr, 'Methods of Strengthening Existing Highway Bridges', Transportation Research Board NCHRP Report (1987) 293.
8. Swamy, R. N., Jones, R. and Bloxham, J. W., 'Structural behaviour of reinforced concrete beams strengthened by epoxy-bonded steel plates', *Struct. Engnr* **65A**(2) (1987) 59–68.
9. Ranisch, E. H. and Rostasy, F. S., 'Bonded steel plates for the reduction of fatigue stresses of coupled tendons in multispan bridges', in 'Adhesion Between Polymers and Concrete', RILEM ISAP 86 (1986) pp. 561–570.
10. Meier, U., 'Bridge repair with high performance composite materials', *Mater. Technik* **4** (1987) 125–128.
11. Saadatmanesh, H. and Ehsani, M., 'Application of fiber-composites in civil engineering', in Proceedings of the sessions related to structural materials at Structures Congress '89, ASCE (1989) pp. 526–535.
12. Kaiser, H., 'Strengthening of Reinforced Concrete with Epoxy-Bonded Carbon-Fiber Plastics', doctoral thesis, ETH, Zurich (1989).
13. L'Hermite, R. and Bresson, J., 'Concrete reinforced with glued plates', in Proceedings of RILEM International Symposium on Synthetic Resins in Building Construction, Paris, 1967, pp. 175–203.
14. Lerchenthal, C. H., 'Bonded steel reinforcement for concrete slabs', *ibid.* pp. 165–173.
15. MacDonald, M. D., 'The Flexural Behaviour of Concrete Beams with Bonded External Reinforcement', TRRL Supplementary Report 415, Transport and Road Research Laboratory, Department of the Environment, Crowthorne, UK, 1978, p. 13.
16. Jones, R., Swamy, R. N., Bloxham, J. and Bouderbalah, A., 'Composite behaviour of concrete beams with epoxy bonded external reinforcement', *Int. J. Cement Compos. Lightwt Concr.* **2**(2) (1980) 91–107.
17. Jones, R., Swamy, R. N. and Ang, T. H., 'Under- and over-reinforced concrete beams with glued steel plates', *ibid.* **4**(1) (1982) 19–32.
18. Ladner, M., 'Reinforced concrete members with subsequently bonded steel sheets', in Proceedings of IABSE Symposium on Strengthening of Building Structures – Diagnosis and Therapy, Venezia, Final Report, Vol. 46 (1983) pp. 203–210.
19. Kent, D. C. and Park, R., 'Flexural members with confined concrete', *J. Struct. Div. ASCE* **97**(7) (1971) 1969–1990.
20. Knott, J. F., 'Fundamentals of Fracture Mechanics' (Butterworths, London, 1973).
21. Anandarajah, A. and Vardy, A. E., 'A theoretical investigation of the failure of open sandwich beams due to interfacial shear fracture', *Struct. Engr* **63B**(4) (1985) 85–92.
22. Triantafillou, T. C. and Gibson, L. J., 'Debonding in foam-core sandwich panels', *Mater. Struct.* **22** (1989) 64–69.
23. Hamoush, S. A. and Ahmad, S. H., 'Debonding of steel plate-strengthened concrete beams', *J. Struct. Engng ASCE* **116**(2) (1990) 356–371.
24. Ladner, M. and Weder, C., 'Concrete Structures with Bonded External Reinforcement', EMPA Report No. 705 (1981).

RESUME

Renforcement de poutres de béton armé par collage (colles époxy) de composites renforcés de fibres

Le renforcement externe de poutres de béton par collage de plastiques renforcés de fibres (FRP) semble un moyen adéquat d'accroître la capacité portante et la rigidité des constructions existantes. Les poutres de béton renforcées de FRP peuvent se rompre de différentes manières quand elles sont chargées en flexion. On identifie et on analyse dans cette étude les processus d'effondrement: fléchissement acier–rupture FRP, fléchissement acier–fragmentation du béton, rupture en compression et décollement.

Nous obtenons ici des équations décrivant chaque mécanisme de rupture en ayant recours à la méthode de déformation compatible, aux concepts de la mécanique de la rupture et à un modèle simple pour le mécanisme du décollement dû aux fissures de cisaillement. Ensuite, nous produisons des diagrammes montrant les calculs de poutre correspondant à chaque mécanisme de rupture, et nous examinons les effets des feuilles de FRP sur les caractéristiques de ductilité et de rigidité des composants renforcés.

En fin de compte, nous donnons les résultats d'essais de flexion quatre points sur des poutres en béton armé renforcées de diverses quantités de feuilles de carbone FRP unidirectionnelles (CFRP). Les résultats confirment l'analyse et soulignent le rôle important de la fissuration dans la délamination de la plaque composite par le processus de décollement. Il apparaît que ce processus impose une limite à l'épaisseur de la feuille composite au-delà de laquelle une rupture fragile se produit, sans que la capacité de flexion soit entièrement réalisée ni la ductilité assurée. On peut utiliser les résultats analytiques obtenus pour établir un processus de sélection de FRP pour le renforcement externe d'éléments de béton par des matériaux légers et durables.